JOURNAL OF GEOPHYSICAL RESEARCH: ATMOSPHERES, VOL. 118, 1679–1689, doi:10.1002/jgrd.50212, 2013

Global precipitation trends in 1900–2005 from a reconstruction and coupled model simulations

Li Ren,[1] Phillip Arkin,[1] Thomas M. Smith,[1,2] and Samuel S.P. Shen[3]

Received 15 October 2012; revised 3 January 2013; accepted 25 January 2013; published 26 February 2013.

[1] The trends of global precipitation in 1900–2005 are evaluated using a historical precipitation reconstruction and coupled model simulations, Coupled Model Intercomparison Project 5 (CMIP5) and Coupled Model Intercomparison Project Phase 3. A significant increasing trend in the global oceanic precipitation is identified in both the reconstruction and models. The trend from the reconstructed ocean precipitation is 0.04 mm day^{-1} over 100a (100 years) and is about twice that of the mean of all models. Over land, the spatial patterns of the trends from both the reconstruction and the models are similar to those shown in the Intergovernmental Panel on Climate Change Fourth Assessment Report. Over the ocean, both reconstruction and models show positive trends in the equatorial and subpolar regions and negative trends over the subtropics. However, the trend magnitude and the locations of the trend peaks are different near the equator (10°S to 10°N) between the reconstruction and the models. CMIP5 future simulations for the global mean project a continuing and stronger precipitation trend in the 21st century than the 20th century.

Citation: Ren L., P. Arkin, T. M. Smith, and S. S. P. Shen (2013), Global precipitation trends in 1900–2005 from a reconstruction and coupled model simulations, *J. Geophys. Res. Atmos.*, *118*, 1679–1689, doi:10.1002/jgrd.50212.

1. Introduction

[2] The Fourth Assessment Report (AR4) of the Intergovernmental Panel on Climate Change (IPCC) reported that since the early 20th century the global mean surface temperature increased by 0.8°C. Theory, model simulations, and observations agree that this surface warming is expected to be and has been accompanied by an increase in atmospheric water vapor [e.g., *Wentz and Schabel*, 2000; *Allen and Ingram*, 2002; *Trenberth et al*., 2005; *Held and Soden*, 2006]. However, precipitation is constrained additionally by the need for condensation heating in the atmosphere to balance with radiative cooling to space [e.g., *Mitchell et al*., 1987; *Allen and Ingram*, 2002]. The amount of change in precipitation associated with a specific amount of change in surface temperature is of critical importance to understanding the global hydrological system and to climate model development and validation. Quantifying the changes of precipitation for the last century can help improve the reliability of projecting the future precipitation variations. Prior studies [e.g. *Adler et al*., 2008; *Wentz et al*., 2007] have been limited since the global precipitation measurements rely on satellite-derived precipitation estimates that have been available only since the late 1970s. IPCC AR4 reported that precipitation has increased over some land areas based on gauge observations [e.g. *Dai et al*., 1997; *Chen et al*., 2002] but did not assess the precipitation trend over the oceans since long-term oceanic precipitation data sets were not available then. In this paper we take advantage of the global reconstructed precipitation data back to 1900 [*Smith et al*., 2012] to quantify the global precipitation trend in the 20th century from observed data.

[3] Only mathematical models of the global climate system are potentially capable of predicting how the behavior of the global water cycle, including the spatial and temporal distribution of precipitation, will change over time as the atmospheric composition of greenhouse gases and aerosols evolves. Coupled models of the atmosphere, ocean, and land surface have been used for several decades to project future climate. Validation of such models relies upon the use of simulations of past climate. The models used in the current generation of future simulations have also been used to simulate, or hindcast, global climate beginning in the 19th century as a part of the Coupled Model Intercomparison Project 5 (CMIP5) [*Whitaker and Hamill*, 2006]. Confidence in these models' projections of the 21st century climate requires improved validation of the skill of their 20th century simulations. In this paper we will evaluate the CMIP5 and Coupled Model Intercomparison Project Phase 3 (CMIP3) [*Meehl et al*., 2007] model simulations of the 20th century precipitation focusing on trends related to changes in anthropogenic forcing to enhance confidence in model-based projections of future climate change.

[4] Our analysis will provide a baseline set of comparisons between model simulations and a variety of

[1]Earth System Science Interdisciplinary Center/Cooperative Institute for Climate and Satellites, University of Maryland, College Park, Maryland, USA.
[2]NOAA/NESDIS/STAR, College Park, Maryland, USA.
[3]San Diego State University, San Diego, California, USA.

Corresponding author: L. Ren, Earth System Science Interdisciplinary Center/Cooperative Institute for Climate and Satellites, University of Maryland, 5825 University Research Court (Ste. 4001), College Park, MD 20740, USA. (lren@umd.edu)

©2013. American Geophysical Union. All Rights Reserved.
2169-897X/13/10.1002/jgrd.50212

observation-based data sets that can be used in model assessments such as the IPCC Fifth Assessment Report (AR5). We will focus on centennial-scale trends of large spatial scales. The model simulations used are those grouped under the label CMIP5 and based on observed historical conditions initialized in 1850. This is an extremely rich data set, and we will generally not emphasize specifics related to individual models or individual members of ensembles. In addition to CMIP5, we will also examine the CMIP3 simulations that were utilized in AR4. The observation-based data set used in this study is the improved reconstructed precipitation of *Smith et al*. [2012].

[5] Evaluation of simulations of large-scale precipitation from global coupled models is challenging as our ability to observe precipitation is limited, making it difficult to determine whether disagreements between models and observations are mainly due to model or observation error. Here we will focus on one aspect of multidecadal precipitation variability: precipitation increases associated with increasing temperatures, under the hypothesis that both observations and models will successfully depict these features. It has been hypothesized that anthropogenic forcing could cause systematic variations in large-scale precipitation associated with global warming. *Arkin et al*. [2010] documented a centennial-scale positive trend in global mean precipitation over the 20th century. Here we move one step further and examine the global mean precipitation trends, zonal means, and spatial patterns using the improved historical precipitation reconstruction of *Smith et al*. [2012], which should have an improved skill in the oceanic long-term variations. We will also compare the precipitation trends from the reconstruction to those in the CMIP5 and CMIP3 models in the 20th century and will conclude by describing the CMIP5 future climate projections in the 21st century in the context of the observed 20th century changes.

[6] Section 2 contains a description of the data sets used in the study. Section 3 examines the long-term trends in observations and models. We will discuss the future projection of the global precipitation trend in CMIP5 models in section 4, and section 5 gives a summary and discussion.

2. Data

[7] Both reconstructed monthly data (as observations) and model data are used for our trend analysis. As there are few observations outside the domain of 75°S to 75°N in the reconstruction [*Smith et al*., 2012], we use this domain for all the calculations described as global, including model data. We define land as any 5° area with greater than 50% being covered by land and ocean as less than 50% being covered by land. There is no 5° area with exactly 50% coverage of land in the land-sea mask obtained from the NOAA Climate Prediction Center.

2.1. Observed Data: Historical Reconstructed Precipitation

[8] A newly developed monthly global reconstructed precipitation (REC) data set beginning in 1900 [*Smith et al*., 2012] is used. This reconstruction used not only the station precipitation data, but also sea level pressure (SLP) and sea surface temperature (SST) data. It can resolve interdecadal global precipitation signals and has improved reliability compared with the previous versions [*Smith et al*., 2008; *Smith et al*., 2009]. Technical improvements include an annual first guess and a station injection procedure. Using output from a canonical correlation analysis (CCA) over the ocean area in the empirical orthogonal function (EOF) reconstruction improves the oceanic representation of multidecadal variations since the CCA uses SST and SLP data as additional information. Although the CCA itself has less skill than gauges, it provides useful skill for multidecadal variations and is used to compensate for a lack of oceanic data in the presatellite period. The CCA is incorporated through an annual first guess analysis using a small number of EOF modes, designed to resolve multidecadal variations. Monthly reconstructions are derived from the annual first guess using monthly increments based on gauge-based EOF modes. Reinjection of gauge data locally improves the land-area analysis of seasonal or shorter-period variations that may not be fully resolved by the reconstruction modes. The spatial resolution is $5° \times 5°$, and the monthly time coverage is from January 1900 to December 2008.

2.2. Modeled Precipitation: CMIP3 and CMIP5

[9] The Coupled Model Intercomparison Project (CMIP) is a platform for comparing global coupled ocean-atmosphere general circulation models developed by a family of modeling centers around the world. It began in 1995 and now is conducted under the auspices of CLIVAR and the Joint Scientific Committee for the World Climate Research Program. The Program for Climate Model Diagnosis and Intercomparison houses the model output contributed by the CMIP modeling groups. CMIP3 began about a decade ago and made model simulations of the 20th–22nd century climate to support AR4. Our analysis selected 24 CMIP3 models with monthly simulations for the period January 1900 to December 1999.

[10] CMIP5 began in September 2008 and uses a new set of coordinated climate model experiments to address outstanding scientific questions that arose from the IPCC AR4 process. It provides modeling support to AR5 and intends to improve understanding of fundamental climate characteristics and provide estimates of future climate change [*Whitaker and Hamill*, 2006]. AR5, scheduled to be published in 2013, will utilize three suites of CMIP5 experiments [*Taylor et al*., 2012]: (a) decadal hindcasts and prediction simulations, (b) "long-term" simulations, and (c) "atmosphere-only" (prescribed SST) simulations. Our trend analysis for the 20th century precipitation uses 25 CMIP5 models with long-term historical experiment (Table 1). The long-term future climate projections of the RCP4.5 experiment in the CMIP5 models are employed in section 4 to describe the 21st century precipitation trend. For that experiment, radiative forcing stabilizes at 4.5 W m^{-2} after 2100. We use the 19 of the 25 models in Table 1 that had RCP4.5 experiment output data available at the time of this study (see Table 1 and section 4 for more details).

[11] Many of the models in CMIP5 (Table 1) have multiple member ensembles available. In this study, we have randomly selected one member for each model. We will not focus on the individual models or ensembles but rather on the mean behavior and variation among models of the 25 CMIP5 models.

Table 1. List of the CMIP5 Models and Modeling Groups That Provided the Data Used in This Paper[a]

Number	Model Name	Modeling Center
1	CCSM4*	NCAR
2	CNRM-CM5*	CNRM-CERFACS
3	CSIRO-MK3.6	CSIRO-QCCCE
4	CanESM2*	CCCMA
5	GFDL-ESM2G*	NOAA-GFDL
6	GFDL-ESM2M*	NOAA-GFDL
7	GFDL-CM3*	NOAA-GFDL
8	GISS-E2-H	NASA-GISS
9	GISS-E2-R*	NASA-GISS
10	HadCM3	MOHC
11	HadGEM2-CC	MOHC
12	HadGEM2-ES*	MOHC
13	IPSL-CM5A-LR*	IPSL
14	IPSL-CM5B-LR*	IPSL
15	MIROC-ESM-CHEM*	MIROC
16	MIROC5*	MIROC
17	MIROC-ESM*	MIROC
18	MPI-ESM-LR*	MPI-M
19	MPI-ESM-P*	MPI-M
20	MRI-CGCM3*	MRI
21	NorESM1-M*	NCC
22	BCC-CSM1.1*	BCC
23	INM-CM4*	INM
24	ACCESS1.0	CSIRO-BOM
25	EC-EARTH	EC-Earth

[a]All the 25 models provided the output for the historical experiments, and the 19 models marked with an asterisk provided the output of the RCP4.5 experiment.

[12] The CMIP3 and CMIP5 model outputs are interpolated onto a common 5° × 5° latitude-longitude grid covering the globe in order to be consistent with REC. The annual anomalies of precipitation are used in the trend analysis. Each annual anomaly is the mean of the year's 12 monthly anomalies, while the monthly climatology for each grid point is calculated as the mean for each month from January to December. The REC monthly climatology is based on the time period 1900 to 2008. The CMIP3 monthly climatology was calculated from 1900 to 1999, and the CMIP5 monthly climatology was calculated from 1900 to 2005.

3. Trends in 20th Century

3.1. REC (1900–2008)

a. Global Average

[13] The global mean annual precipitation anomalies of REC (Figure 1) indicate a general increasing tendency over both land and ocean from 1900 to 2008. The trend over land is 0.03 mm day^{-1} per 100a (100 years), which is slightly weaker than that over the oceans (0.04 mm day^{-1} per 100a). Over the ocean (Figure 1), the interannual variations (dashed line) are mostly associated with warm and cold phases of ENSO variations. The global mean annual mean anomalies including both land and ocean in REC precipitation variations are generally correlated with the temperature variations over the century with the temporal correlation of 0.60. Such correlation increases to 0.80 with 9 year Gaussian filtering and decreases to 0.28 after de-trending, which suggests that the correlation between the global precipitation and surface temperature is dominated by the long-term trend but does include some correspondence on shorter time scales. The surface temperature data used here are the HadCRUT3 from the Climate Research Unit (CRU) [*Brohan et al.*, 2006; *Rayner et al.*, 2006]. The hydrological sensitivity, which represents the change in global mean precipitation for a 1° increase in global mean surface temperature [*Arkin et al.*, 2010], is 2.1% K^{-1} from REC, using a global average

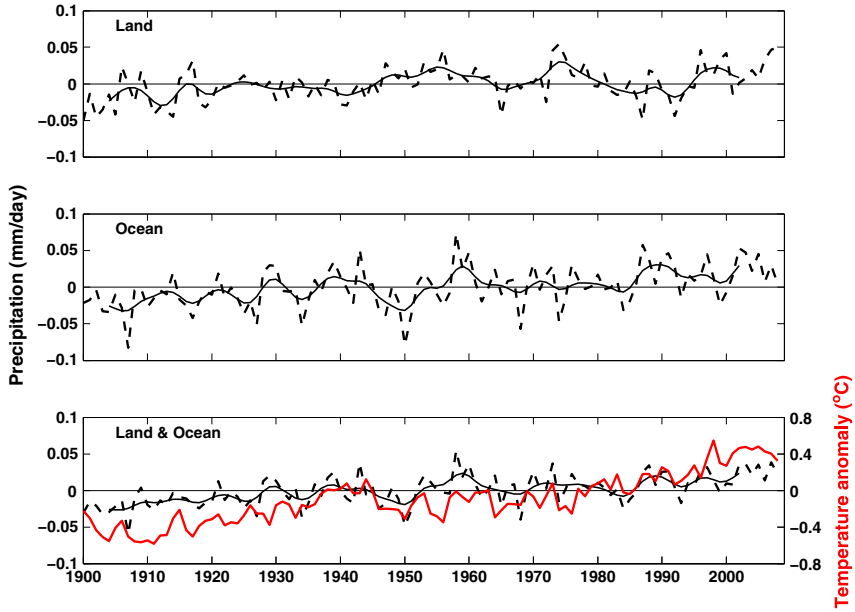

Figure 1. Annual and global (75°S to 75°N) averaged REC anomalies from 1900 to 2008 over the land, ocean, and land and ocean areas. The dashed lines are the annual mean anomalies, and the solid black lines are smoothed values calculated using nine-point Gaussian filter. The red line is the global average annual mean anomalies of surface temperature from 1900 to 2008. The temperature data are the HadCRUT3 from CRU. The trend in the temperature is 0.7°C per 100a.

precipitation of 2.67 mm day^{-1} (GPCP 1979–2008) and the warming trend of 0.7°C per century. This number is similar to that estimated by *Held and Soden* [2006] which is 2.2% K^{-1} from AR4 simulations in the 20th century. *Arkin et al.* [2010] obtained 2.5% K^{-1} based on an earlier version of reconstruction of [*Smith et al.*, 2009].

b. Zonal Means Over Oceans

[14] The trends along latitudes averaged over the oceans (Figure 2) show very strong positive trends in the equatorial regions between 5°N and 15°N, which are likely dominated by the Intertropical Convergence Zone (ITCZ) [*Barry and Chorley*, 1992]. Negative trends exist in the northern subtropics from 15°N to 30°N and between 20°S and 40°S in the Southern Hemisphere. The mixture of positive and negative trend distributions shown in Figure 3a in these regions implies another level complexity. Over the subpolar oceans, both the Northern Hemisphere (north of 30°N) and the Southern Ocean (south of 40°S) show strong positive trends.

[15] The zonal distribution of the reconstructed precipitation trends is consistent with the documented ocean salinity changes [e.g., *Durack and Wijffels*, 2010; *Wong et al.*, 1999] that show a decrease of salinity in the equatorial and subpolar regions and an increase of salinity in the subtropical regions. Also documented is an intensification of the hydrological cycle over the past 50 years [e.g., *Durack et al.*, 2012; *Hosoda et al.*, 2009; *Roemmich and Gilson*, 2009]. Here, the zonal distribution of the reconstruction precipitation trends over the ocean suggests a likely strengthening of the hydrological cycle over the past 100 years. Although there is no other documentation of the long-term trend in the entire 20th century over oceanic areas, the consistency of the zonally averaged trends in salinity and the oceanic precipitation qualitatively supports the reconstruction.

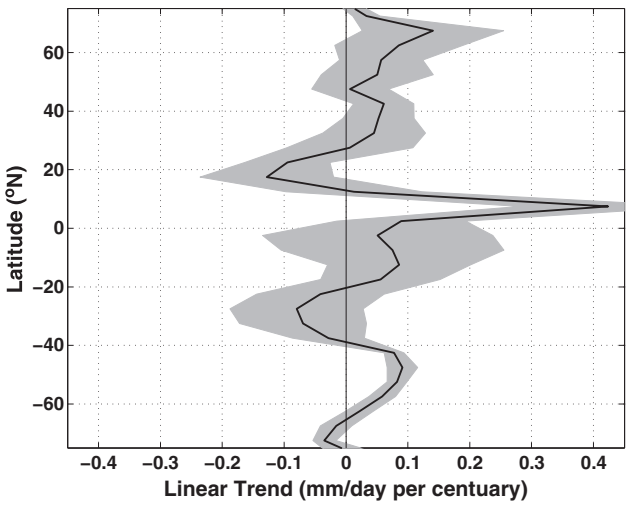

Figure 2. The zonally averaged annual mean precipitation anomaly trends of the historical precipitation reconstruction over the oceans. The trends (solid line) were calculated from the zonally averaged annual mean precipitation anomaly trends during the time period 1900 to 2008. The shaded gray area illustrates the confidence interval of the trends along the latitudes at 95% confidence level using Student *t* test.

c. Spatial Patterns

[16] Over the lands, the spatial distribution of the trend estimated from the annual mean anomalies (Figure 3a) has variations similar to the IPCC AR4 Figure 3.13 (trend in annual precipitation from 1901 to 2005), which is not surprising since the REC reinjected the GHCN data. Positive trends, largely weak, were observed over much of North America (except Southwest United States), Amazonia and southeastern South America, much of Eurasia, and northern Australia; negative trends are observed across northern Africa and much of eastern South America.

[17] Over the oceans, the annual mean anomaly trends (Figure 3a) show the greatest increases in the eastern tropical Pacific and most of the Indian Ocean. Increasing trends were also observed in the northeastern and western Pacific, the north Atlantic, and much of the Southern Ocean. The largest negative trends appeared in the west equatorial Pacific Ocean and most of the subtropics in both Pacific and Atlantic Oceans. A positive/negative couplet is found in the region of the South Pacific Convergence Zone [*Kiladis et al.*, 1989].

[18] Since long-term changes in large-scale precipitation are hypothesized to be related to the background mean state [e.g., *Allan and Soden*, 2008; *Chou et al.*, 2009], trends in different seasons should differ from each other and from the overall annual mean trend. We examine the long-term trends in December-January-February (DJF) and June-July-August (JJA) (Figures 3b and 3c). Over the lands, the trends in DJF are negative over most of the U.S., Western India, and parts of eastern Asia, but neutral to positive over these regions in JJA. Trends in DJF are positive over Bangladesh, Myanmar, southern South America, and northwest Australia, but negative over these regions in JJA. Over the oceans, the trends differ most in the tropical regions (30°N–30°S) in DJF and JJA. Trends in DJF are positive in majority of the Indian Ocean, but negative in JJA in the eastern Indian Ocean. Trends in DJF are neutral in the tropical Atlantic Ocean, but a positive/negative couplet extends from east Brazil to West Africa in JJA. Trends in DJF are negative in the west equatorial Pacific and positive in JJA. In extratropical regions (outside of 30°N–30°S), the patterns of the trends are similar in DJF and JJA with stronger signals in the winter season.

3.2. Models

[19] The examination of global precipitation trends in the 20th century from the REC provides the foundation of our understanding of the trends. As future climate projections rely on coupled climate model simulations, the assessment of coupled model simulations of trends in the past century helps establish confidence in future projections. Here both CMIP5 and CMIP3 are examined and compared with the REC results for trends in the global averages, zonal oceanic averages, and spatial patterns in the 20th century. Twenty-five CMIP5 (Table 1) and 24 CMIP3 models are used in this paper.

a. Global Averages

[20] The global means of the annual mean precipitation anomalies in most of the models in CMIP5 and CMIP3 have

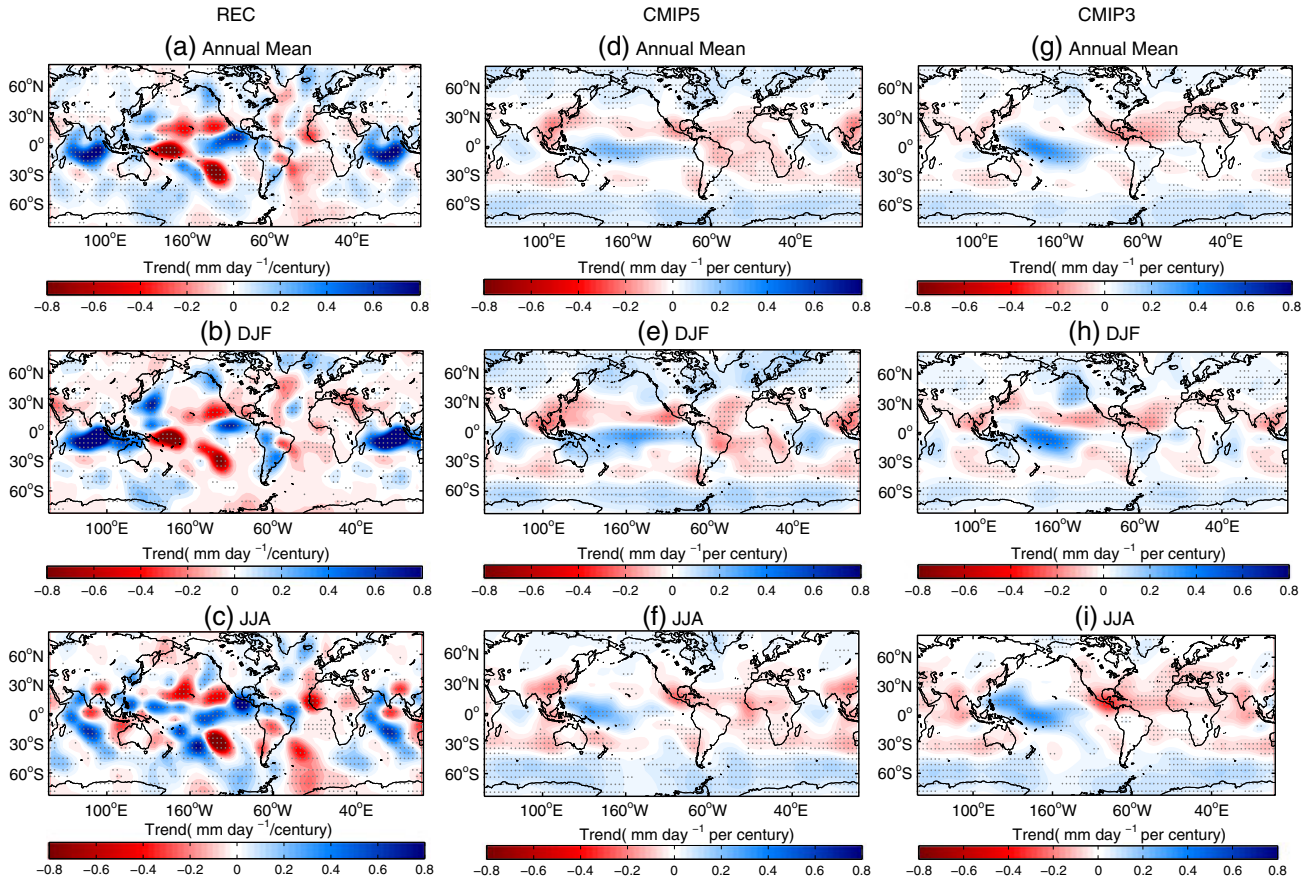

Figure 3. Spatial distribution of the precipitation linear trend. (a) REC annual mean trend, (b) REC DJF trend, (c) REC JJA trend, (d) CMIP5 annual mean trend, (e) CMIP5 DJF trend, (f) CMIP5 JJA trend, (g) CMIP3 annual mean trend, (h) CMIP3 DJF trend, and (i) CMIP3 JJA trend. The linear trends were calculated from the annual mean anomalies for the annual mean trend, mean anomalies from December, January, and February for DJF and mean anomalies from June, July, and August for JJA. In REC, the gray dot represents the locations where the trends being estimated from the linear regression are significantly different from zero at 5% confidence level. The gray dot in CMIP5 and CMIP3 represents the locations where the mean trends among the models are different from zeros using Student *t* test at 95% confidence level. Units are mm day^{-1} per 100a.

an increasing tendency over oceans (Figure 4). The mean trend over the ocean is 0.02 mm day^{-1} per 100a in CMIP3 and CMIP5 models. They are both weaker than our observation-based reconstruction, consistent with the findings of *Durack et al*. [2012] who found an intensified global water cycle from the ocean salinity observations in the past 50 years at a rate stronger than those in the CMIP3 models. Neither CMIP5 nor CMIP3 models show significant trends over land. The global mean annual mean precipitation anomalies in individual models over the land have larger variations than over the ocean in both CMIP5 and CMIP3 (Figures 4a and 4b), with an average standard deviation of 0.032 mm day^{-1} over land and 0.021 mm day^{-1} over oceans in CMIP5, and 0.037 mm day^{-1} over land and 0.021 mm day^{-1} over oceans in CMIP3. However, the variations in REC over the oceans are larger than over land with lower standard deviation over land (0.023 mm day^{-1}) than over oceans (0.028 mm day^{-1}). Although the reasons for stronger variations over land are clear in the models, the larger oceanic variations in REC are unclear. These variance results are consistent for both CMIP5 and CMIP3.

[21] In CMIP5 models, the global precipitation anomaly averages show significant drops in 1902, 1963, 1982, and 1991 (Figure 4a) over both land and ocean. Those drops are coincident with and presumably associated with the aerosols resulting from the volcanic eruptions of Pelee/Sourfiere/Santa Maria, Agung, El Chichon, and Pinatubo in 1902, 1963, 1982, and 1991, respectively. The CMIP3 models show weaker volcanic signals (Figure 4b). Whether a significant volcanic signal exists in precipitation is still in debate [e.g., *Mass and Portman*, 1990; *Gu and Adler*, 2011]. The volcanic effects on global precipitation may lessen the trends in the CMIP5 models. For example, more than 3 years after the 1963 Agung event, global precipitation over both land and ocean still had not recovered to the pre-eruption state, which suggests that the model volcanic aerosols remain in the atmosphere longer than in nature, reducing the global precipitation accordingly.

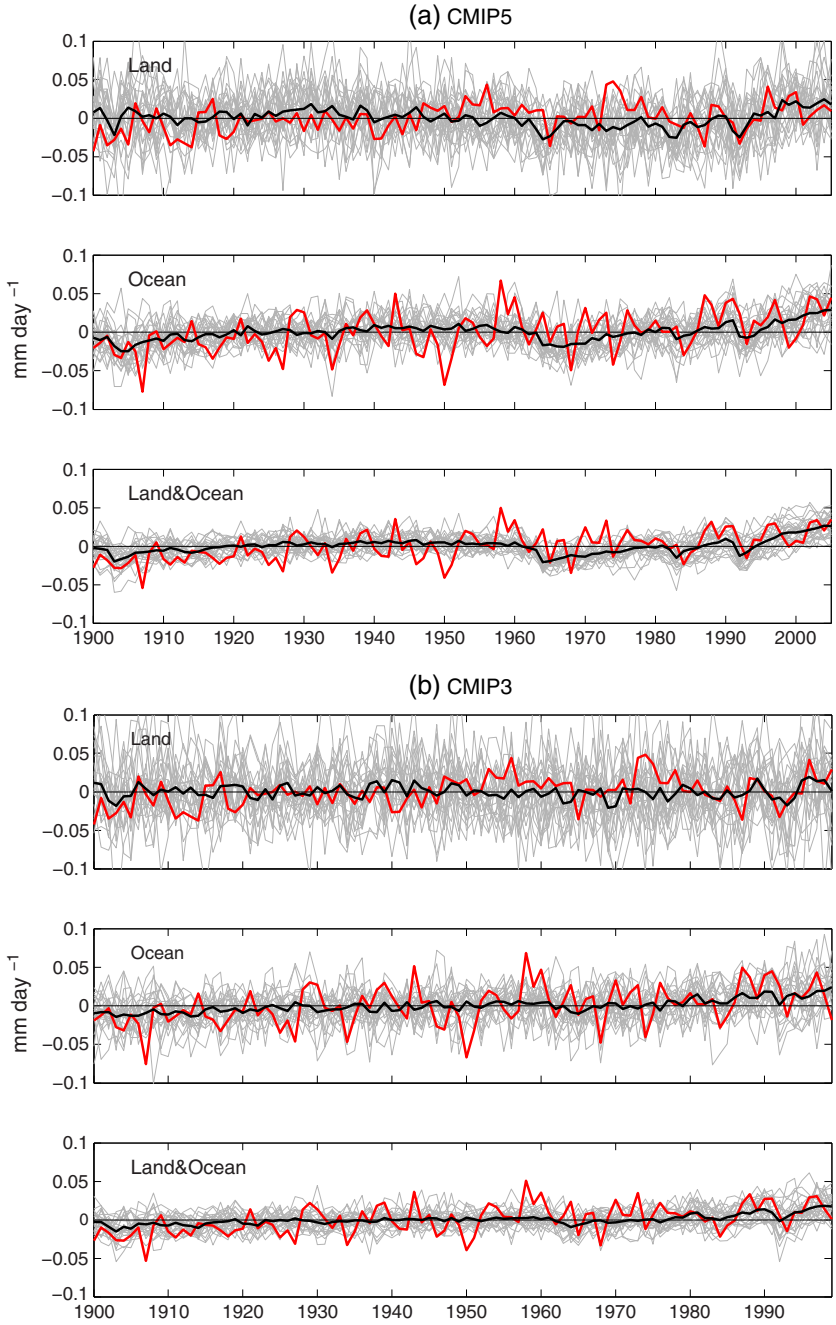

Figure 4. Annual and global (75°S to 75°N) average of precipitation anomaly (mm day^{-1}) in the 25 models in (a) CMIP5 and 24 models in (b) CMIP3 for land, ocean, and land and ocean. Each model is plotted using gray lines; the black line is the mean of all the models, and the red line is the global average annual mean anomalies of REC.

[22] We computed the time series correlations between the global averages of precipitation anomalies of REC and each CMIP5 and CMIP3 model (Figure 5). The correlations indicate that the models are better correlated with the REC over ocean than over land. Also, the correlations over the oceans have a broader range in both CMIP5 and CMIP3 than over lands. The 25th percentile of the correlations (bottom of the box) is higher in CMIP5 than CMIP3 over the oceans (Figure 5). Also, the 2nd percentile of the correlations over the globe in CMIP5 is higher than that in CMIP3. These findings are not affected by removing the trends, although the correlation values are reduced (not shown).

b. Zonal Means Over Oceans

[23] The zonal averages of the trends in most of the models in CMIP5 and CMIP3 are consistent with significant positive trends in the equatorial and subpolar oceans and significant negative trends in the subtropical oceans (Figure 6), indicating a strengthening of the hydrological cycle. Both CMIP3 and CMIP5 have similar latitude distributions of the

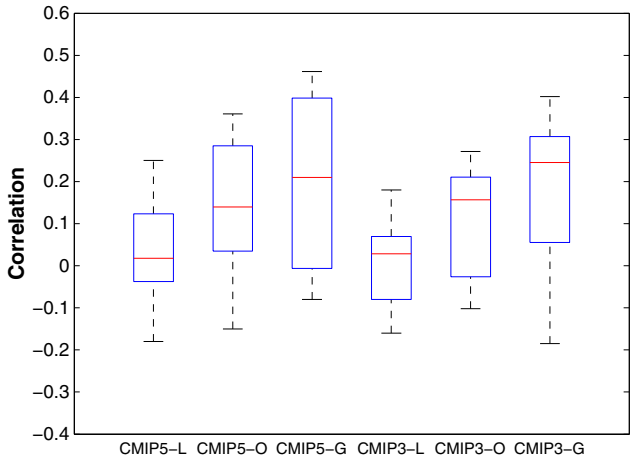

Figure 5. Boxplot of the correlations of global mean annual mean precipitation anomalies between each CMIP5 and CMIP3 model run and the REC over land (L), ocean (O), and the globe (G). The box ranges show the scatter of the correlation between different models to REC. Red lines mark the medians, the bottom of the box is the 25th percentile, the top of the box is the 75th percentile, and lines extending from the top of the boxes are the 98th percentile and from the bottom of the boxes are the 2nd percentile.

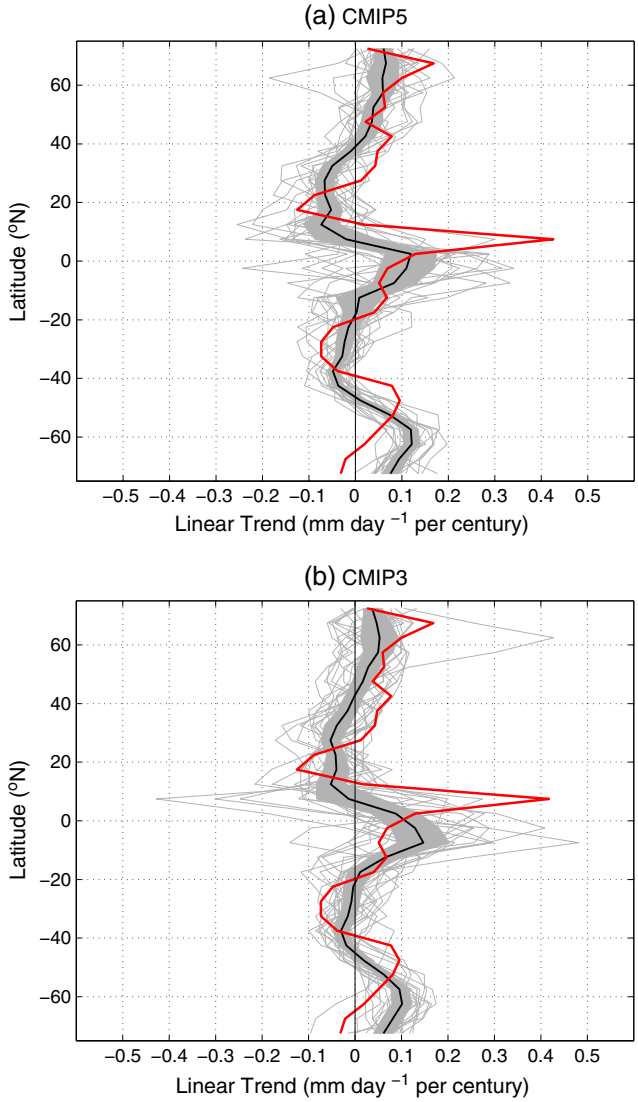

Figure 6. The zonally averaged annual precipitation trends over the oceans: (a) CMIP5 and (b) CMIP3. The red lines are for the REC. The faint gray lines show the zonally averaged trends along the latitudes for each individual model, and the black line is the mean of the models. The shaded gray area illustrates the 95% confidence interval of the trends among different models using Student *t* test.

trends. The trends of zonal averages from the REC are similar to the models but with some noticeable differences. In the tropical oceans, REC positive trends are shifted further north compared to the models. In the subtropical oceans, the models show a negative trend in 5°N–40°N and 20°S–45°S, while REC shows negative trends in 10°N–25°N and 20°S–40°S. In the subpolar oceans, the models have positive trends north of 40°N and south of 45°S, while REC trends are positive north of 25°N and south of 40°S.

[24] The seasonality of the zonal averaged trends in CMIP5 and CMIP3 models shows similar features, and only CMIP5 is shown in Figure 7. Many similarities in the zonal averaged seasonal trends are found in the CMIP5 models and REC. In DJF (Figure 7a), the zonal averaged trends generally intensify the gradient of zonal distribution of the total precipitation in both CMIP5 and REC. In JJA (Figure 7b), the trends likely expand the ITCZ in the models and REC. Additionally, both the subtropical minimum and mid-latitude storm track tend to shift poleward in the Southern Hemisphere. The subtropical minimum becomes drier due to the negative trends in the Northern Hemisphere.

c. Spatial Patterns

[25] The spatial distributions of the mean trends estimated from the annual mean precipitation anomalies in the 25 CMIP5 models (Figure 3d) show some resemblance to trends in the REC (Figure 3a). On large scales, CMIP5 models exhibit high latitude increases, subtropical decreases, and increases in the equatorial Pacific and Indian Ocean (Figure 3d). The greatest difference between REC and the averaged trends among the models appears in the equatorial Pacific Ocean. The REC is less uniform than the models, likely due to the averaging of 25 models. In addition, due to the averaging, the magnitudes of the trends in Figure 3d are weaker than those in Figure 3a, but the magnitude of the trends for each individual model is similar as the REC. The spatial patterns of the trends for individual models generally replicate the large-scale patterns in Figure 3d; however, differences among models do exist, particularly in the tropics (not shown).

[26] The linear correlations of the spatial patterns between the REC and the mean of the 25 CMIP5 are low (~0.02) possibly due to the differences in the equatorial Pacific Ocean and the magnitudes. For example, the correlation increases to 0.2 if the magnitudes of the trends are ignored by setting the positive trends as 1 and negative trends as −1. Therefore, the models capture the large spatial scale and the signs of the global trends in the 20th century. CMIP3 models have similar features. Both the similarities and the differences

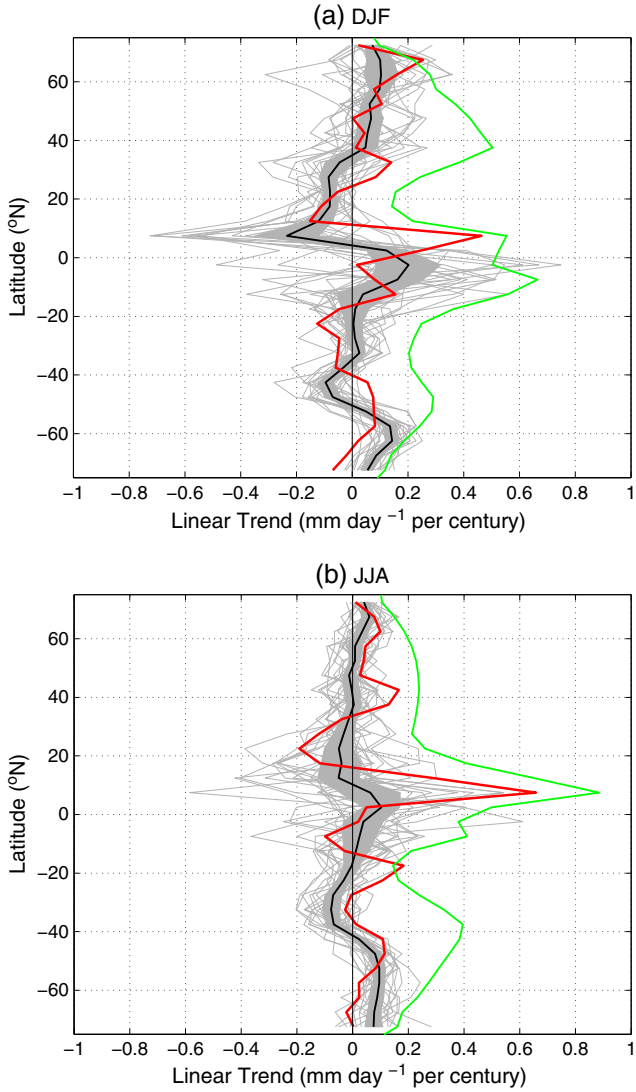

Figure 7. The zonally averaged annual precipitation trends over the oceans of the 25 CMIP5 models and the REC (red lines) in different seasons: (a) DJF and (b) JJA. The faint gray lines show individual models in CMIP5, the black line is the mean of the models, and the shaded gray area illustrates the 95% confidence interval of the mean trends among different models using Student's *t* test. The green lines are the zonal mean of the climatology from CMIP5 in DJF and JJA.

between the models and the REC, particularly the differences, are important and need further investigation.

[27] The long-term trends in DJF and JJA of the CMIP5 ensemble means are shown in Figures 3e and 3f, respectively. On large scales, the increasing trends at high latitudes in the Northern Hemisphere and Indian Ocean are stronger in DJF than in JJA. The decreasing trends in subtropical regions, particularly the North Pacific Ocean, are stronger in DJF than in JJA. Additionally, the increasing trends in the west equatorial Pacific Ocean are farther north in JJA, and the increasing trends in the east equatorial Pacific are weaker in JJA.

[28] The CMIP3 and CMIP5 spatial patterns of the annual mean anomaly trends are similar and have minor differences in the equatorial Pacific, where the CMIP3's positive trend tilts southward from west to east (Figure 3g), while CMIP5's positive trend is zonally distributed (Figure 3d). Also, the 25 models in CMIP5 agree better with each other than the 24 models in CMIP3. Therefore, a larger region shows significant trends in Figure 3d, which includes western Europe, South Africa, the Indian Ocean, and the west basin of the subtropical North Pacific Ocean. The trends in these regions are all consistent with the trends in the REC (Figure 3a), which suggests that the trends in CMIP5 have better agreements with REC than CMIP3. In CMIP3, The DJF positive trends in the northeast Pacific Ocean, equatorial Atlantic Ocean, central and west of South American and West Indian Ocean in the DJF season are neutral or positive in JJA (Figures 3h and 3i). On large scales, the positive trends over the high latitude in the Northern Hemisphere and most of the equatorial latitude bands except the Pacific Ocean in DJF are weaker or neutral in JJA. The seasonal differences between DJF and JJA are very similar in CMIP3 and CMIP5 model runs.

4. Future Projections: Trends in 21st Century

[29] The examination of the 20th century precipitation trends from models and observations suggests that global precipitation has increased, particularly over oceanic areas. Although the spatial distribution of the trends varies from region to region in a complex fashion, the zonal averages show a consistent increase over the equatorial and subpolar oceans and a decrease over the subtropics. As CMIP5 simulations has a better agreement with the reconstruction for the global precipitation trends in the 20th century, in this section, 19 CMIP5 models in Table 1 (marked with an asterisk) with output from the RCP4.5 experiment from January 2006 to December 2010 are used to analyze the projected precipitation trend of the global average and spatial patterns in the 21st century.

[30] The global-annual precipitation anomalies (Figure 8) from all the 19 models indicate increases over the ocean and land, and globally from 2006 to 2100. The mean trend is 0.13 mm day^{-1} per 100a over the oceans, 0.10 mm day^{-1} per 100a over the lands, and 0.13 mm day^{-1} per 100a globally. The global oceanic trend is slightly higher than the global land trend, and such features in the projection are similar to those in the 20th century from REC, CMIP3, and CMIP5. However, the trends projected in the 21st century by the 19 models are roughly an order of magnitude stronger than both the observed and simulated trends in the 20th century.

[31] The spatial distribution of the annual mean precipitation anomaly trends estimated from CMIP5 models for the 21st century (2006–2100) shows that the models agree with each other in most of the positive trend regions (blue areas of Figure 9). Over the land, the increasing trends appear in the eastern and western North America, eastern and southern Asia, and northern Europe. In the tropical oceans, the precipitation in the 21st century shows a significant positive trend in the Pacific and Indo-Pacific equatorial regions. In the subtropics, significant negative trends appear in the eastern basin in the Southern Hemisphere where climatological precipitation is low. Positive trends in the Northern Hemisphere subtropical regions are weaker. Also, significant positive trends exist over the entire Southern Ocean. The Northern Hemisphere high-latitude regions are dominated by positive trends as well.

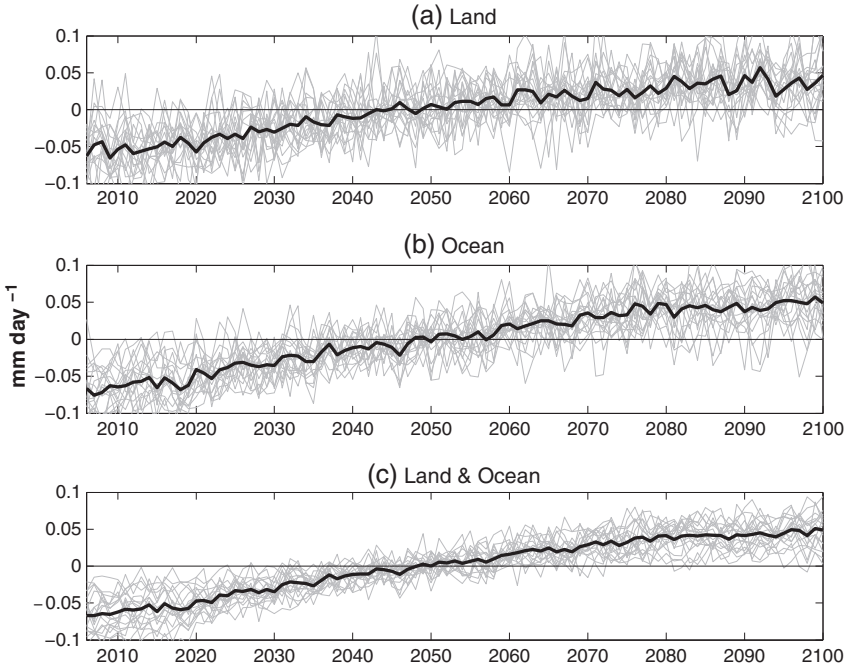

Figure 8. Annual and global (75°S to 75°N) average of precipitation anomaly (mm day^{-1}) in the 19 CMIP5 models with the faint gray line being individual 19 CMIP5 models and the black line being the mean of the 19 models: (a) land, (b) ocean, and (c) land and ocean.

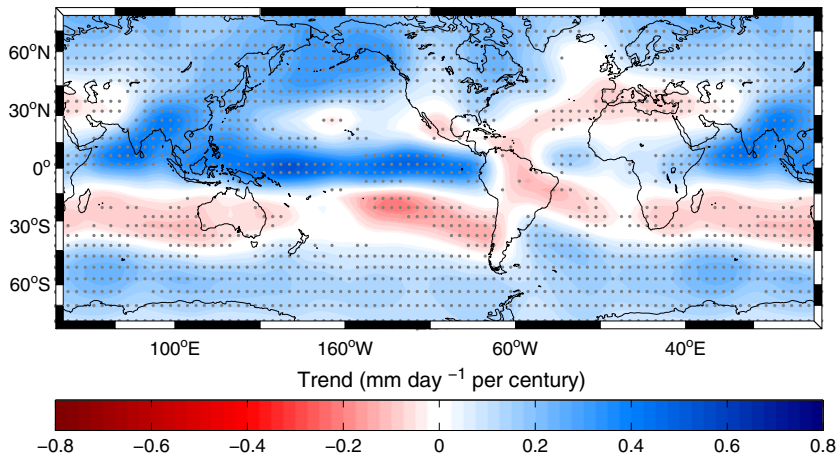

Figure 9. The spatial distribution of the trends estimated as the mean among the 19 CMIP5 models from 2006 to 2100 with the gray dots locating the regions where the mean trends among the 19 models are different from zeros using Student's *t* test at 95% confidence level.

[32] In most areas with significant precipitation trends in the 20th century (Figures 3a, 3d, and 3g), the projected precipitation in the 21st century also have the same features, e.g., positive trends in the majority of the U.S., East Asia, and Southern Oceans, and negative trends over the southern subtropical oceans, especially over the eastern parts of those regions.

5. Summary and Discussion

[33] The precipitation trends from REC, CMIP5, and CMIP3 in the 20th century (1900 to 2005) are summarized using global averages, zonal mean over oceans, and spatial patterns.

a. Global Averages

[34] The global-annual mean precipitation anomalies over the 20th century show a significant positive trend over the oceans in REC, CMIP3, and CMIP5 and a significant trend over land only in REC. Over the oceans, REC has the largest trend, and the trends in both CMIP3 and CMIP5 are about half of the size. Over land, neither CMIP3 nor CMIP5 has a significant trend. Compared to REC, both CMIP3 and CMIP5 have consistent but slightly weaker oceanic trends. The volcanic signals in CMIP3 models are weaker than those in CMIP5 models.

b. Zonal Means Over Oceans

[35] The latitudinal distribution of oceanic precipitation trends generally shows positive trends in the equatorial and subpolar regions and negative trends in the subtropical regions (Figures 2 and 6). The CMIP3 and CMIP5 models agree well with each other for those zonal features. REC shows more latitude variations than the models. As shown in the spatial maps (Figure 3), they do not agree over the tropics. Consequently, latitudinal distribution of the trends in the tropics shows large differences. However, the seasonality of the zonal mean anomalies (Figure 7) shows consistent features between the REC and the models. In DJF, they both show an intensification of the gradient of zonal distribution of the total precipitation (green line). In JJA, they both show that ITCZ is expanding, and the subtropical minimum and mid-latitude storm track in the Southern Hemisphere both shift poleward. In the Northern Hemisphere, the subtropical minimum becomes drier.

c. Spatial Patterns

[36] The spatial patterns of the annual mean anomaly trends in REC, CMIP5, and CMIP3 are generally consistent, particularly the CMIP3 and CMIP5 (Figures 3a, 3d, and 3g). CMIP5 agrees better with REC than CMIP3. For example, positive trends over the tropical Indian Ocean occur in REC and CMIP5, although weaker in CMIP5, but there are no significant trends over this region in CMIP3. There is poor agreement of the spatial patterns over the equatorial oceans between REC and the models, particularly in the tropical Pacific Ocean.

[37] There are seasonal variations in the spatial distribution of the trends in REC, CMIP5, and CMIP3. The nontrivial differences exist mostly in the high latitudes of the Northern Hemisphere, Indian Ocean, and equatorial Pacific and Atlantic Ocean.

[38] The 19 CMIP5 models used to evaluate the RCP4.5 experiment agree with each other in projecting future precipitation trends. The global mean of the precipitation anomalies is projected to continue increasing with an accelerating trend (Figure 8) over the 21st century. The oceanic areas including equatorial and subpolar regions are projected to be generally dominated by positive trends, and the subtropical regions, particularly the eastern basins of subtropical oceans, will be dominated by negative trends (Figure 9). Those projected changes could influence oceanic circulation by altering near-surface density and surface winds implied by systematic precipitation changes. For example, lower rainfall over subtropical semipermanent high-SLP zones implies increasing SLP, which could lead to intensification of oceanic circulation associated with that pressure zone. Less precipitation would also lead to greater surface density, also contributing to enhanced circulations. Those circulations are important to the mid-latitude climate, and any systematic alteration on them could cause systematic climate changes. The long-term precipitation trends' impact on the global ocean circulation will be explored in a separate paper.

[39] Over the land (Figure 9), the precipitation over most of the U.S., northern Europe, and East Asia is projected to increase in the 21st century. However, the southwest U.S. and northeast South America are projected to have continued decreasing precipitation. This has implications for fresh water availability over these regions and could pose serious challenges to sustained habitability in those regions.

[40] Significant warming in surface temperatures has already occurred, and both theory and models project continuation of that trend in the future. This warming is hypothesized to impact the global hydrological cycle, including precipitation, but until recently, the limited observational data for oceanic precipitation have not been adequate to validate model simulations. In this paper we take advantage of our global precipitation reconstruction [*Smith et al*., 2012] covering the time period from 1900 to 2008 to describe the observed trend in global precipitation and to compare it to simulations from the CMIP3 and CMIP5 models to confirm their large-scale results during the 20th century. Significant increasing trends of global mean precipitation were found in both the reconstruction and the model simulations, and the zonal means of the trends over the oceans in both the reconstruction and models consistently show increasing trends in the equatorial and subpolar regions and decreasing trends in the subtropics. The degree of agreement between the reconstruction and model simulations in both the mean change and its latitudinal distribution over the oceans increases confidence in both, and is an initial step toward the validation of regional climate simulations of changes in precipitation.

[41] **Acknowledgments.** We acknowledge the World Climate Research Programme's Working Group on Coupled Modelling, which is responsible for CMIP, and we thank the climate modeling groups (listed in Table 1 of this paper) for producing and making available their model output. For CMIP, the U.S. Department of Energy's Program for Climate Model Diagnosis and Intercomparison provides coordinating support and has led development of software infrastructure in partnership with the Global Organization for Earth System Science Portals. This work is supported by the U.S. National Science Foundation (Awards No. AGS-1015926 and AGS-1015957). Li Ren's work is also supported by NASA Ocean Salinity Science Team (NNX09AU74G). Phillip Arkin's work is partially supported by the NOAA Cooperative Institute for Climate and Satellite (NA09NES4400006).

References

Adler, R. F., G. J. Gu, J. J. Wang, G. J. Huffman, S. Curtis, and D. Bolvin (2008), Relationships between global precipitation and surface temperature on interannual and longer timescales (1979–2006), *J. Geophys. Res.-Atmos.*, *113*.

Allan, R. P., and B. J. Soden (2008), Atmospheric warming and the amplification of precipitation extremes, *Science*, *321*(5895), 1481–1484.

Allen, M. R., and W. J. Ingram (2002), Constraints on future changes in climate and the hydrologic cycle, *Nature*, *419*(6903), 224–+.

Arkin, P. A., T. M. Smith, M. R. P. Sapiano, and J. Janowiak (2010), The observed sensitivity of the global hydrological cycle to changes in surface temperature, *Environ. Res. Lett.*, *5*(3).

Barry, R. G., and R. J. Chorley (1992), Atmosphere, Weather and Climate, London.

Brohan, P., J. J. Kennedy, I. Harris, S. F. B. Tett, and P. D. Jones (2006), Uncertainty estimates in regional and global observed temperature changes: A new data set from 1850, *J. Geophys. Res.-Atmos.*, *111*(D12).

Chen, M. Y., P. P. Xie, J. E. Janowiak, and P. A. Arkin (2002), Global land precipitation: A 50-yr monthly analysis based on gauge observations, *J. Hydrometeorol.*, *3*(3), 249–266.

Chou, C., J. D. Neelin, C. A. Chen, and J. Y. Tu (2009), Evaluating the "rich-get-richer'' mechanism in tropical precipitation change under global warming, *J. Climate*, *22*(8), 1982–2005.

Dai, A., I. Y. Fung, and A. D. DelGenio (1997), Surface observed global land precipitation variations during 1900–88, *J. Climate*, *10*(11), 2943–2962.

Durack, P. J., and S. E. Wijffels (2010), Fifty-year trends in global ocean salinities and their relationship to broad-scale warming, *J. Climate*, *23*(16), 4342–4362.

Durack, P. J., S. E. Wijffels, and R. J. Matear (2012), Ocean salinities reveal strong global water cycle intensification during 1950 to 2000, *Science*, *336*(6080), 455–458.

Gu, G. J., and R. F. Adler (2011), Precipitation and temperature variations on the interannual time scale: Assessing the impact of ENSO and volcanic eruptions, *J. Climate*, *24*(9), 2258–2270.

Held, I. M., and B. J. Soden (2006), Robust responses of the hydrological cycle to global warming, *J. Climate*, *19*(21), 5686–5699.

Hosoda, S., T. Suga, N. Shikama, and K. Mizuno (2009), Global surface layer salinity change detected by Argo and its implication for hydrological cycle intensification, *J. Oceanogr.*, *65*(4), 579–586.

Kiladis, G. N., H. Vonstorch, and H. Vanloon (1989), Origin of the South-Pacific Convergence Zone, *J. Climate*, *2*(10), 1185–1195.

Mass, C. F., and D. A. Portman (1990), Major volcanic-eruptions and climate - A critical-evaluation - Reply, *J. Climate*, *3*(5), 589–590.

Meehl, G. A., C. Covey, T. Delworth, M. Latif, B. McAvaney, J. F. B. Mitchell, R. J. Stouffer, and K. E. Taylor (2007), The WCRP CMIP3 multimodel dataset - A new era in climate change research, *B. Am. Meteorol. Soc.*, *88*(9), 1383–+.

Mitchell, J. F. B., C. A. Wilson, and W. M. Cunnington (1987), On Co2 climate sensitivity and model dependence of results, *Q. J. Roy. Meteor. Soc.*, *113*(475), 293–322.

Rayner, N. A., P. Brohan, D. E. Parker, C. K. Folland, J. J. Kennedy, M. Vanicek, T. J. Ansell, and S. F. B. Tett (2006), Improved analyses of changes and uncertainties in sea surface temperature measured in situ sice the mid-nineteenth century: The HadSST2 dataset, *J. Climate*, *19*(3), 446–469.

Roemmich, D., and J. Gilson (2009), The 2004–2008 mean and annual cycle of temperature, salinity, and steric height in the global ocean from the Argo Program, *Prog. Oceanogr.*, *82*(2), 81–100.

Smith, T. M., M. R. P. Sapiano, and P. A. Arkin (2008), Historical reconstruction of monthly oceanic precipitation (1900–2006), *J. Geophys. Res.-Atmos.*, *113*(D17).

Smith, T. M., P. A. Arkin, and M. R. P. Sapiano (2009), Reconstruction of near-global annual precipitation using correlations with sea surface temperature and sea level pressure, *J. Geophys. Res.-Atmos.*, *114*.

Smith, T. M., P. A. Arkin, L. Ren, and S. S. P. Shen (2012), Improved reconstruction of global precipitation since 1900, *J. Atmos. Ocean. Tech.*, *29*(10), 1505–1517.

Taylor, K. E., R. J. Stouffer, and G. A. Meehl (2012), An overview of CMIP5 and the experiment design, *B. Am. Meteorol. Soc.*, *93*(4), 485–498.

Trenberth, K. E., J. Fasullo, and L. Smith (2005), Trends and variability in column-integrated atmospheric water vapor, *Clim. Dynam.*, *24*(7–8), 741–758.

Wentz, F. J., and M. Schabel (2000), Precise climate monitoring using complementary satellite data sets, *Nature*, *403*(6768), 414–416.

Wentz, F. J., L. Ricciardulli, K. Hilburn, and C. Mears (2007), How much more rain will global warming bring?, *Science*, *317*(5835), 233–235.

Whitaker, J. S., and T. M. Hamill (2006), Ensemble data assimilation without perturbed observations. (vol 130, pg 1313, 2002), *Mon. Weather. Rev.*, *134*(6), 1722–1722.

Wong, A. P. S., N. L. Bindoff, and J. A. Church (1999), Large-scale freshening of intermediate waters in the Pacific and Indian oceans, *Nature*, *400*(6743), 440–443.